Setup of three Mach-Zehnder interferometers for production and observation of Greenberger-Horne-Zeilinger entanglement of electrons

A. A. Vyshnevyy,[1] G. B. Lesovik,[2] T. Jonckheere,[3,4] and T. Martin[3,4]

[1]*Department of General and Applied Physics, MIPT, Institutskiy per. 9, 141700 Dolgoprudnyy, Moscow Region, Russia*

[2]*L. D. Landau Institute for Theoretical Physics RAS, Kosygina str. 2, 119334 Moscow, Russia*

[3]*Aix Marseille Université, CNRS, CPT, UMR 7332, 13288 Marseille, France*

[4]*Université de Toulon, CNRS, CPT, UMR 7332, 83957 La Garde, France*

We propose a new single-step scheme for the generation of a Greenberger-Horne-Zeilinger (GHZ) entangled state of three single-electron excitations (flying qubits). We also present a method to get a generalized GHZ state. Our idea relies upon the most recent progress in the field of on-demand electron sources and mesoscopic Mach-Zehnder interferometry. We also provide the recipe for the unambiguous detection of this GHZ state via correlation measurements at the output, which imply the violation of a Bell-type inequality which is generalized to the case of three particles. We explain how such measurements can be achieved in the context of Mach-Zehnder interferometry and draw an actual prototype device which could be achieved with point contacts and metallic gates placed on a GaAs sample, in the integer quantum Hall effect regime.

I. INTRODUCTION

Quantum entanglement, first noted by Einstein-Podolsky-Rosen (EPR)[1] and Schrödinger,[2] is a genuine property of quantum mechanics. Qualitative embodiment of this property was given by Bell,[3] who showed that entangled states have stronger correlations than allowed by local hidden variable theories (LHVTs). Later Clauser and coworkers[4] suggested a more transparent inequality (B-CHSH), the violation of which was experimentally demonstrated for photons.[5]

During the last decade, several works have been achieved in the context of mesoscopic physics to explore two-particle entanglement. The initial proposals used superconducting sources of electrons connected to two normal metal leads, through which the two constituent electrons originating from a Cooper pair were split to form a singlet state outside the superconductor.[6,7] Other proposals for two-electron entanglement were subsequently made using ballistic electrons and point contacts placed in the integer quantum Hall effect (IQHE) regime.[8,9] Bell inequality tests based on stationary current noise cross correlations revealed that a maximal violation could be achieved.[8–13]

In the context of quantum optics, Greenberger, Horne, and Zeilinger introduced a maximally entangled tripartite state, commonly called the GHZ state.[14] The Bell parameter in the tripartite case can take values up to 4, while the corresponding parameter in the bipartite case is no more than $2\sqrt{2}$.[15] For both cases the LHVT limit remains 2. In this sense the entanglement is considered to be "stronger" than for the two-particle state, and it is thus potentially easier for experimental detection. Reference 14 pointed out that the measurement results for this state are in conflict with local realism when quantum mechanics makes definite (nonstatistical) predictions, in contrast with EPR states. The GHZ state has a number of potential applications in quantum information. It can be used for quantum error correction,[16] and it was proved that tripartite states have advantages compared

to bipartite ones in quantum teleportation[17] and in dense coding.[18] There are two established methods to produce entangled states of electrons. The first method exploits the indistinguishability of fermions and relies on postselection to get the desired entangled state[19] (see also Ref. 20 for a discussion of the role of projection in this case). The second way is to use the interaction between particles (application of this method with flying electronic qubits is described in Refs. 21–23). The latter has the advantage that the evolution during the preparation of the state is unitary and thus can be deterministic, with up to 100% efficiency for producing the desired state.

While various ways exist to create and manipulate entangled states of qubits in optical systems[5,24,25] and NMR (nuclear magnetic resonance) experiments,[26] in mesoscopic systems the generation of an experimentally determined entangled state of few electrons and the subsequent proof that Bell inequalities have successfully violated both represent a considerable challenge. A proposal which follows faithfully the quantum optics experimental protocol[19] uses edge states in the IQHE and achieves the GHZ state using postselection.

The purpose of the present work is to go beyond this existing protocol and thus to explore three-particle orbital entanglement with ballistic electrons propagating in mesoscopic devices using the interaction between electrons. This proposal is motivated by the recent progress in achieving single-electron sources[27] and for building effective electron Mach-Zehnder interferometers (MZIs).[28]

The outline of the paper is as follows. In Sec. II, we describe the three-MZI setup and specify how the beam splitters (BSs) and Coulomb interaction operate. In Sec. III we justify that a GHZ state is produced at the outcome. In Sec. IV we describe the Bell inequality test, which is used to show that maximal entanglement is achieved. In Sec. V we implement this test for our three- MZI device. In Sec. VI we show a possible realization of our setup in the IQHE regime. We conclude in Sec. VII.
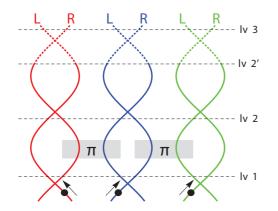
FIG. 1. (Color online) Proposed setup for the creation of an electronic GHZ state. Three MZIs interferometers (solid lines), coupled by Coulomb interactions (π boxes). Three electrons are injected simultaneously into the three MZIs and propagate from the bottom to the top. The crossing of the lines indicates a beam splitter (BS), where an electron can exit in one of the two output branches. The dotted lines for each MZI show a third BS, used to explainthe detection process theoretically. Dashed horizontal lines specify different levels of the setup, which are used in the theoretical explanations.

II. DESCRIPTION OF THE SETUP

A schematic of the device is depicted in Fig. 1. It consists of three MZIs, which are placed side by side (shown by solid lines in Fig. 1). Each MZI consists of two incoming channels, which meet at the first BS. The two outgoing channels from this BS propagate and meet at the second BS. The theoretical setup also has a second loop (shown by dotted lines in Fig. 1), with propagation from the output channels of the second BS, and recombination at a third BS. We use this second loop to explain theoretically the detection of the GHZ states, and we show in Sec. V that it is possible in practice to get rid of this second loop and perform the GHZ-state production and detection with a single loop.

We distinguish the right (R) and left (L) sides of each interferometer and label single-electron-wave functions accordingly. For instance, at any stage of the wave-packet evolution, ψ_{jC} denotes an electron wave packet on the C side ($C = R, L$) of the jth MZI ($j = 1, 2, 3$).

The most likely candidates for electron channels are edge states in the IQHE regime, which have the advantage that they are immune to backscattering effects by impurities and have a long phase breaking time. Several experiments involving MZIs in the IQHE have already been performed,[28] some of them involving setups with two MZIs. A proposal for a detailed setup is given in Sec. VI. We assume that a single-electron wave packet is emitted in each MZI above the Fermi sea. Such single-electron emission was recently demonstrated experimentally with an on-demand single-electron source[27,29] which uses the mesoscopic capacitor as the injector. The BSs are assumed to be reflectionless, i.e., incident particles cannot be backscattered in the same channel; they can only be transmitted farther "up" (in Fig. 1). The BS can be
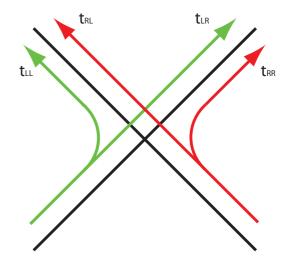

FIG. 2. (Color online) Reflectionless beam splitter with transition amplitudes.

parametrized by a transfer matrix,

$$T = \begin{pmatrix} t_{RR} & t_{LR} \\ t_{RL} & t_{LL} \end{pmatrix} = \begin{pmatrix} i\sin\theta & \cos\theta \\ \cos\theta & i\sin\theta \end{pmatrix}, \quad (1)$$

which relates incoming states to outgoing states; θ is the transparency parameter (see Fig. 2). For example, if $\theta = 0$ the BS is transparent, meaning that the incident particle goes from R to L and from L to R without scattering, while for $\theta = \pi/4$ the incident particle may appear in each of the output channels with equal probability, $1/2$. There exists an additional freedom in choosing the phases of scattering matrix elements but it does not affect the results in a crucial manner (see Appendix B for details). Here we specify the bottom BSs to have equal probability, $1/2$, for transmission in the R and L side channels ($\theta = \pi/4$). The transfer matrix is then simply

$$T = \begin{pmatrix} i/\sqrt{2} & 1/\sqrt{2} \\ 1/\sqrt{2} & i/\sqrt{2} \end{pmatrix}. \quad (2)$$

This choice of the bottom BSs as well as the π phase shift in the Coulomb interaction is analogous to that in studies[21–23] of two MZIs. In each of them a maximally entangled bipartite state was achieved when the first row of BSs was half-reflecting.

The main steps in the production of the GHZ state are as follows. The first stage is the synchronized injection of electrons (filled circles with arrows at the bottom in Fig. 1), which then pass through the first BS of each of the three MZIs. Beyond the first BS, free propagation occurs for electrons wave packets, until they reach the "interaction region": the L channel of the first MZ and the R channel of the second MZ and, separately, the L channel of the second MZ and the R channel of the third MZI are put in close proximity so that Coulomb interaction effects between the two pairs of neighboring channels become important. The effective length of this interaction region is such that it generates an overall π phase shift of the two-particle wave functions associated with the two neighboring channels. It may be unclear why Coulomb interaction would produce a phase shift because the Coulomb interaction involves an energy exchange process.
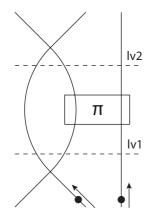
FIG. 3. Illustration of the analogy between an MZI and a spin counter: one MZI coupled to a lead via Coulomb interaction (see text for details).

This matter and conditions required for the phase shift to be produced are discussed in Appendix E. After the interaction region the three electrons propagate freely towards the second BS, but we allow the insertion of a phase difference Φ in each MZ loop. The phase differences which are needed here could be achieved via the Aharonov-Bohm (AB) effect or via a scalar potential. Actually, AB and Coulomb interaction phase accumulation occur together but logically the process can be decoupled into a sequence of independent processes. From this point of view the AB phase effectively changes the transfer matrix of the following BS (see Appendix B), which is convenient for further calculations. The final stage in our setup is the measurement of the state of the three particles in the output arms (top of Fig. 1).

To understand the role of the interaction regions, let us consider first a given MZI with an electron injected into the right lead (see Fig. 3). The electron in this interferometer can be treated as a "flying qubit," i.e., a two-state system, where states are specified by the side chosen in the interferometer, where the electron travels. The initial state therefore is ψ_R. After the bottom BS, at level "lv1" (see Fig. 3), the state of the electron is

$$\Psi = \frac{1}{\sqrt{2}}(i\psi_R + \psi_L). \tag{3}$$

Next, we add a wire coupled to the interferometer with an electron injected simultaneously. So the initial state is $\psi_{1R}\psi_2$. When two electrons pass the interaction zone they accumulate mutual phase π. After interaction the two-particle state remains separable, and each particle has a wave function. If the interaction occurs, we get at level "lv2" for the left electron:

$$\psi_\pi = \frac{1}{\sqrt{2}}(-i\psi_{1R} + \psi_{1L}). \tag{4}$$

If we do not inject an electron into the right lead, then at level lv2 we have, for the left electron,

$$\psi_0 = \frac{1}{\sqrt{2}}(i\psi_{1R} + \psi_{1L}). \tag{5}$$

These two outcomes are orthogonal to each other, $\langle\psi_0|\psi_\pi\rangle = 0$, thus we can distinguish cases when zero or one electron travels in the neighboring lead. Moreover, the relation
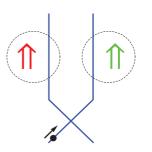

FIG. 4. (Color online) The three-MZI setup (up to lv2) represented in terms of spin counters: because of the interaction regions, the left and right MZIs in Fig. 1 act like spin counters (large arrows here) coupled to the left and right wires of the middle MZI.

$\langle\psi_0|\psi_\pi\rangle = 0$ is universal in the sense that it is preserved when we change the lead where electrons are injected into the MZI or when we place the wire to the left of the MZI (as long as the bottom BS remains half-reflecting). We may put in correspondence with the wave function ψ_0 a qubit state $|\Uparrow\rangle$, and with ψ_π a state $|\Downarrow\rangle$. This makes our three-MZI setup very similar to the situation displayed in Fig. 4. There we have a spin-based electron counter with spin flipping after one electron passes through a wire (as described in Ref. 30). This analogy between the MZI and the spin-based counter described here is helpful for understanding the nature of the GHZ state in the proposed setup (Fig. 1).

Up to level lv2 in Fig. 1, the evolution can be represented in terms of spin counters (Fig. 4). After passing through the BS the electron state in the middle MZI is $\psi = \frac{1}{\sqrt{2}}(\psi_R + i\psi_L)$. Depending on the arm from which the electron came, the corresponding spin flips. This produces the final state,

$$\Psi = \frac{1}{\sqrt{2}}(|\Uparrow\rangle\psi_R|\Downarrow\rangle + i|\Downarrow\rangle\psi_L|\Uparrow\rangle), \tag{6}$$

which is obviously a GHZ-type state.

III. GHZ-STATE PRODUCTION

A. Standard GHZ-state production

We give here a detailed explanation of the GHZ-state production. We find an exact expression for the electron state at level lv2 in Fig. 1, and we identify the local unitary transform, making it a standard GHZ state. "Local" means that the unitary transform is a direct product of three unitary operators each acting over a Hilbert space of a corresponding electron, $U = U_1 \otimes U_2 \otimes U_3$.

Specifically the initial three-particle state is chosen to be (see bottom of Fig. 1):

$$\psi = \psi_{1R}\psi_{2L}\psi_{3L}. \tag{7}$$

Note that we choose a simple product state, instead of choosing a Slater determinant of the three single-particle wave functions. This is due to the fact that the electron wave functions do not have mutual parts of trajectories, so that exchange effects do not play any considerable role.

At level lv1, after passing the first row of BSs,

$$\Psi = \frac{1}{2^{3/2}}(\psi_{1L} + i\psi_{1R})(\psi_{2R} + i\psi_{2L})(\psi_{3R} + i\psi_{3L}). \tag{8}$$

In order to determine the state after the Coulomb interaction has acted, we rewrite the previous equation as

$$\Psi = \frac{1}{2\sqrt{2}}(\psi_{1L} + i\psi_{1R})\psi_{2R}(\psi_{3R} + i\psi_{3L})$$
$$+ \frac{1}{2\sqrt{2}}(\psi_{1L} + i\psi_{1R})i\psi_{2L}(\psi_{3R} + i\psi_{3L}). \quad (9)$$

The state after interaction (at lv2),

$$\Psi = \frac{1}{2\sqrt{2}}(\psi_{1L} + i\psi_{1R})\psi_{2R}(\psi_{3R} - i\psi_{3L})$$
$$+ \frac{1}{2\sqrt{2}}(\psi_{1L} - i\psi_{1R})i\psi_{2L}(\psi_{3R} + i\psi_{3L}), \quad (10)$$

or, in a more symmetrical way,

$$\Psi = \frac{1}{2\sqrt{2}}(\psi_{1L} + i\psi_{1R})(-i)\psi_{2R}(i\psi_{3R} + \psi_{3L})$$
$$+ \frac{1}{2\sqrt{2}}(i\psi_{1L} + \psi_{1R})\psi_{2L}(\psi_{3R} + i\psi_{3L}). \quad (11)$$

Now it is easy to see the unitary transformation which produces the canonical GHZ state,

$$\Psi_{\text{GHZ}} = \frac{1}{\sqrt{2}}(\psi_{1R}\psi_{2R}\psi_{3R} + \psi_{1L}\psi_{2L}\psi_{3L}), \quad (12)$$

from Eq. (11). It should transform $\frac{1}{\sqrt{2}}(\psi_{1L} + i\psi_{1R})$ into ψ_{1R}, $\frac{i}{\sqrt{2}}(\psi_{1L} - i\psi_{1R})$ into ψ_{1L}, $-i\psi_{2R}$ into ψ_{2R}, ψ_{2L} into ψ_{2L}, $\frac{1}{\sqrt{2}}(\psi_{3R} - i\psi_{3L})$ into ψ_{3R}, and $\frac{1}{\sqrt{2}}(\psi_{3R} + i\psi_{3L})$ into ψ_{3L}. This transform is

$$U = U_1 \otimes U_2 \otimes U_3, \quad (13)$$

where

$$U_1 = U_3 = \frac{1}{\sqrt{2}}\begin{pmatrix} -i & 1 \\ 1 & -i \end{pmatrix}, \quad U_2 = \begin{pmatrix} i & 0 \\ 0 & 1 \end{pmatrix}. \quad (14)$$

So, at level lv2 of our setup (Fig. 1) we have the GHZ state up to a change of basis achieved by the transform, Eq. (14). This transform could be performed by the second BS row between level lv2 and level lv2′. As one may notice, transformation U_2 does not correspond to any θ parameter in the formula for the transfer matrix of BS, (1). We may avoid this problem by choosing $\theta = \frac{\pi}{2}$ and shifting the AB phase in the next MZ loop by $\frac{\pi}{2}$. In reality we do not need this action because we intend to use the "condensed" scheme, where preparation and measurement are performed with one row of the BSs (see Sec. V B).

It is interesting to note that, from the quantum computation point of view, we have an algorithm implemented on three flying qubits which is essentially similar to the coding scheme depicted in Fig.10.2. of Nielsen-Chuang.[16]

B. Generalized GHZ-state production

In this work we stay focused on the creation of a GHZ state in its original form, $|\Psi\rangle = \frac{1}{\sqrt{2}}(|\uparrow\uparrow\uparrow\rangle + |\downarrow\downarrow\downarrow\rangle)$. However, in some cases it might be useful to obtain a more general GHZ-type state such as $|\Psi\rangle = a|\uparrow\uparrow\uparrow\rangle + b|\downarrow\downarrow\downarrow\rangle$ with arbitrary a and b. Such a generalized state could be useful, e.g., for quantum error correction.[16] In our setup it is possible to get

such a GHZ-type state by a slight modification of the method presented above. We simply need to replace the half-reflecting BS in the second MZI with another one. As we pointed out earlier in the general case the transfer matrix of the BS can be represented as follows:

$$T = \begin{pmatrix} i\sin\theta & \cos\theta \\ \cos\theta & i\sin\theta \end{pmatrix}. \quad (15)$$

With this BS in the second MZI the electronic wave function is

$$\psi = \cos\theta|\Uparrow\rangle\psi_R|\Downarrow\rangle + i\sin\theta|\Downarrow\rangle\psi_L|\Uparrow\rangle), \quad (16)$$

which is a generalized GHZ state in a "rotated" basis. Using the same unitary transformation $U = U_1 \otimes U_2 \otimes U_3$, where U_i are defined in Eq. (14), produces the generalized GHZ state in its canonical form.

IV. BELL-TYPE INEQUALITY FOR THREE PARTICLES

To detect the GHZ state experimentally we suggest using a Bell-type inequality violation test for three particles.[31] Let us discuss some basic facts about Bell-type inequalities for three particles, which constitute one of the possible generalizations of the Bell inequality in a tripartite case.

We start from an algebraic inequality,

$$|B| = |x_1' x_2 x_3 + x_1 x_2' x_3 + x_1 x_2 x_3' - x_1' x_2' x_3'| \leqslant 2, \quad (17)$$

which is satisfied when x_1, x_2, x_3, x_1', x_2', and x_3' are real variables with absolute values $\leqslant 1$ (this is a three-particle generalization of the algebraic inequality used for Bell inequality tests on two particles).

Consider a three-particle entangled state, written in pseudospin notation ($R = \uparrow$, $L = \downarrow$; each particle can be detected in one of two leads, L and R). The projection of the pseudospin of j on some vector $\mathbf{a_j}$ corresponds to x_j, while the projection on $\mathbf{a_j'}$ corresponds to x_j'. From the point of view of LHVTs, after the creation of the three-particle state, between the two measurements the first electron has projections $\sigma_{\mathbf{a_1}}$ and $\sigma_{\mathbf{a_1'}}$; the second one, $\sigma_{\mathbf{a_2}}$ and $\sigma_{\mathbf{a_2'}}$; and the third one, $\sigma_{\mathbf{a_3}}$ and $\sigma_{\mathbf{a_3'}}$ ($\sigma_{\mathbf{a_1}} = 1$ if the spin is parallel to $\mathbf{a_1}$, and $\sigma_{\mathbf{a_1}} = -1$ if it has the opposite direction). Different outcomes of measurements are due to a hidden variable ξ which varies from measurement to measurement. We have identified the real numbers x_1, x_1', x_2, x_2', x_3, x_3' with $\sigma_{\mathbf{a_1}}(\xi)$, $\sigma_{\mathbf{a_1'}}(\xi)$, $\sigma_{\mathbf{a_2}}(\xi)$, $\sigma_{\mathbf{a_2'}}(\xi)$, $\sigma_{\mathbf{a_3}}(\xi)$, $\sigma_{\mathbf{a_3'}}(\xi)$. The average value of B is then given by

$$\bar{B} = \int \left(\sigma_{\mathbf{a_1'}}\sigma_{\mathbf{a_2}}\sigma_{\mathbf{a_3}} + \sigma_{\mathbf{a_1}}\sigma_{\mathbf{a_2'}}\sigma_{\mathbf{a_3}} + \sigma_{\mathbf{a_1}}\sigma_{\mathbf{a_2}}\sigma_{\mathbf{a_3'}} - \sigma_{\mathbf{a_1'}}\sigma_{\mathbf{a_2'}}\sigma_{\mathbf{a_3'}} \right)$$
$$\times \rho(\xi)d\xi, \quad (18)$$

where $\rho(\xi)$ is the distribution function of the hidden variable. Experimentally this value can be measured by the following procedure. Let us define the correlator,

$$E(\mathbf{a_1 a_2 a_3}) = \langle \sigma_{\mathbf{a_1}}\sigma_{\mathbf{a_2}}\sigma_{\mathbf{a_3}} \rangle \equiv \int \sigma_{\mathbf{a_1}}\sigma_{\mathbf{a_2}}\sigma_{\mathbf{a_3}}\rho(\xi)d\xi. \quad (19)$$

Then

$$\bar{B} = E(\mathbf{a_1'}, \mathbf{a_2}, \mathbf{a_3}) + E(\mathbf{a_1}, \mathbf{a_2'}, \mathbf{a_3}) + E(\mathbf{a_1}, \mathbf{a_2}, \mathbf{a_3'})$$
$$- E(\mathbf{a_1'}, \mathbf{a_2'}, \mathbf{a_3'}), \quad (20)$$

and from Eq. (17) the local hidden variable average is such that

$$\bar{B} \leqslant 2. \qquad (21)$$

From a quantum mechanical point of view, the correlator of Eq. (19) is an average over the state of an operator describing the measurement of three spins in specific directions,

$$E(\mathbf{a_1}, \mathbf{a_2}, \mathbf{a_3}) = \langle \hat{\sigma}_{\mathbf{a_1}} \otimes \hat{\sigma}_{\mathbf{a_2}} \otimes \hat{\sigma}_{\mathbf{a_3}} \rangle, \qquad (22)$$

and

$$\bar{B} = \langle \hat{B} \rangle, \qquad (23)$$

where the analog of the "Bell operator" for three particles reads

$$\hat{B} = \hat{\sigma}_{\mathbf{a_1'}} \otimes \hat{\sigma}_{\mathbf{a_2}} \otimes \hat{\sigma}_{\mathbf{a_3}} + \hat{\sigma}_{\mathbf{a_1}} \otimes \hat{\sigma}_{\mathbf{a_2'}} \otimes \hat{\sigma}_{\mathbf{a_3}}$$
$$+ \hat{\sigma}_{\mathbf{a_1}} \otimes \hat{\sigma}_{\mathbf{a_2}} \otimes \hat{\sigma}_{\mathbf{a_3'}} - \hat{\sigma}_{\mathbf{a_1'}} \otimes \hat{\sigma}_{\mathbf{a_2'}} \otimes \hat{\sigma}_{\mathbf{a_3'}}. \qquad (24)$$

In Appendix A we recall under which conditions this Bell operator gives a maximal violation of the Bell-type inequality. The demonstration is based on the fact that, first, in order for $\hat{B}^2$ to have an eigenvalue equal to 16, the state must be a linear superposition of $|\uparrow\uparrow\uparrow\rangle$ and $|\downarrow\downarrow\downarrow\rangle$. Second, the Bell operator $\hat{B}$ has eigenvalues ± 4 only if the state is related to the GHZ state,

$$\Psi \equiv \frac{1}{\sqrt{2}} (|\uparrow\uparrow\uparrow\rangle + |\downarrow\downarrow\downarrow\rangle), \qquad (25)$$

by local unitary transformations. Finally, in Appendix A, we specify which angles of spin measurement give the maximal value for $\bar{B}$. The resulting angles are

$$\mathbf{a_1} = \begin{pmatrix} \cos\phi_{\mathbf{a_1}} \\ \sin\phi_{\mathbf{a_1}} \\ 0 \end{pmatrix}, \quad \mathbf{a_1'} = \begin{pmatrix} \cos(\phi_{\mathbf{a_1}} \pm \pi/2) \\ \sin(\phi_{\mathbf{a_1}} \pm \pi/2) \\ 0 \end{pmatrix},$$

$$\mathbf{a_2} = \begin{pmatrix} \cos\phi_{\mathbf{a_2}} \\ \sin\phi_{\mathbf{a_2}} \\ 0 \end{pmatrix}, \quad \mathbf{a_2'} = \begin{pmatrix} \cos(\phi_{\mathbf{a_2}} \pm \pi/2) \\ \sin(\phi_{\mathbf{a_2}} \pm \pi/2) \\ 0 \end{pmatrix}, \quad (26)$$

$$\mathbf{a_3} = \begin{pmatrix} \cos\phi_{\mathbf{a_3}} \\ \sin\phi_{\mathbf{a_3}} \\ 0 \end{pmatrix}, \quad \mathbf{a_3'} = \begin{pmatrix} \cos(\phi_{\mathbf{a_3}} \pm \pi/2) \\ \sin(\phi_{\mathbf{a_3}} \pm \pi/2) \\ 0 \end{pmatrix},$$

where $\phi_{\mathbf{a_1}} + \phi_{\mathbf{a_2}} + \phi_{\mathbf{a_3}} = \mp\pi/2$ (different signs identify two classes of angles corresponding to the upper and lower signs in the formulas). The origin of these classes lies in the symmetry of the GHZ state with respect to reflection in the x-y plane. These angles will further be transformed into the corresponding BS parameters, θ and Φ.

V. DETECTION SCHEME

A. Detailed detection scheme

We are now in a position to describe all the steps for production and detection, which are achieved in a rather complicated three-MZI setup, with each MZI containing double loops (Fig. 1). The incoming state of Eq. (7) is injected into the first BS and becomes that of Eq. (8) at level lv1. The π shift is applied to neighboring channels and it results in the rotated GHZ state of Eq. (11) at level lv2. The true GHZ state of Eq. (12) is achieved at level lv2′ by passing through

the second BS row (with phase shift). The next MZI loop is associated with the Bell measurement process.

To produce the Bell measurement correlator we need three values, x_1, x_2, and x_3, corresponding to separate measurements with results within the band $[-1; 1]$. In the spin case, the spin projection measurements serve this purpose. In our setup we can detect a particle in the left or in the right arm. So one of the possible assignments is $x = -1$ for a particle detected in the left arm and $x = 1$ for a particle detected in the right arm. Then the Bell correlator is the average of the product $x_1 x_2 x_3$, which, by definition, is

$$E = \langle x_1 x_2 x_3 \rangle = 1 * P_1 + (-1) * P_{-1}, \qquad (27)$$

where P_1 is the probability for $x_1 x_2 x_3$ to be equal to 1, and P_{-1} to -1, correspondingly. $x_1 x_2 x_3 = 1$ in four cases. The first is $x_1 = 1$, $x_2 = 1$, $x_3 = 1$, which corresponds to the case where the three electrons were observed in the right arms. We define the probability of this event as P_{RRR}. The other three possible cases have corresponding probabilities $P_{LLR}, P_{LRL}, P_{LLR}$. So

$$P_1 = P_{RRR} + P_{LLR} + P_{LRL} + P_{RLL}. \qquad (28)$$

Analogously,

$$P_{-1} = P_{LLL} + P_{RRL} + P_{RLR} + P_{LRR}. \qquad (29)$$

Finally,

$$E = \langle x_1 x_2 x_3 \rangle = P_{RRR} + P_{RLL} + P_{LRL} + P_{LLR}$$
$$- P_{LLL} - P_{LRR} - P_{RLR} - P_{RRL}. \qquad (30)$$

This correlator measured on level "lv3" of the setup in Fig. 1 corresponds to the $\langle \hat{\sigma}_z \otimes \hat{\sigma}_z \otimes \hat{\sigma}_z \rangle$ correlator of the pseudospin.

1. Measurement of pseudospin in arbitrary directions

As we have seen in Sec. III, in order to make Bell measurements we should be able to measure pseudospin projections in arbitrary directions, say, $\mathbf{n}$. Nevertheless, it cannot be achieved directly because we can only measure the presence of the particles in the right or the left lead ("spin up-spin down"). Instead one can do an equivalent measurement which gives the same expectation values. One should transform the state in such a way that the direction $\mathbf{n}$ of the pseudospin converts to z and then perform the standard measure procedure, Eq. (30). This is done by the upper BSs, and we obtain $\langle \hat{\sigma}_{\mathbf{n_1}} \otimes \hat{\sigma}_{\mathbf{n_2}} \otimes \hat{\sigma}_{\mathbf{n_3}} \rangle$ for the state on level lv2′. The relation between rotation parameters and BS characteristics is described in Appendix B. For each Bell correlator the parameters of this loop are different. As soon as we have defined the correlators $E(\mathbf{a_1'}, \mathbf{a_2}, \mathbf{a_3})$, $E(\mathbf{a_1}, \mathbf{a_2'}, \mathbf{a_3})$, $E(\mathbf{a_1}, \mathbf{a_2}, \mathbf{a_3'})$, and $E(\mathbf{a_1'}, \mathbf{a_2'}, \mathbf{a_3'})$ we are ready to calculate the value of the Bell observable,

$$B = E(\mathbf{a_1'}, \mathbf{a_2}, \mathbf{a_3}) + E(\mathbf{a_1}, \mathbf{a_2'}, \mathbf{a_3}) + E(\mathbf{a_1}, \mathbf{a_2}, \mathbf{a_3'})$$
$$- E(\mathbf{a_1'}, \mathbf{a_2'}, \mathbf{a_3'}), \qquad (31)$$

which is the result of the experiment.

Granted, the fact that we have to include an additional loop in each MZI is quite cumbersome and renders the implementation of our setup with mesoscopic devices more difficult. In the next section we show that it is possible to perform the same task without the additional loop.

B. Condensed detection scheme

Here, we insist that the use of an additional loop in each MZ can be circumvented, provided that we exploit the composition of two BS in series. We call the setup where the additional loop has been removed the "condensed detection scheme." Consider one of three interferometers (Fig. 1). After level lv2 it has two BSs, each performing its own unitary transformation. Let the transformation matrices of the BS located between level lv2 and level lv2′ and the BS between lv2′ and lv3 be U and V, correspondingly. Then the total transformation UV is also unitary. The idea is to perform this total transformation with a single BS and, thus, to keep the setup as simple as possible (i.e., remove the dotted-line part of Fig. 1).

To be precise, note that a single BS cannot reproduce fully all unitary transformations, and there is the possibility that the transform UV cannot be reproduced in full generality with a single BS. But it can be shown that, from the *point of view of measurement*, it is always possible with a single BS to perform a transformation which gives the same measure as the total transformation UV. We leave the details of the proof of this statement to the appendixes (in particular, Appendix D).

It is interesting to note that in the condensed detection setup, there exists a measurement scheme where the desired violation $B = 4$ is achieved using only changes of the phase difference Φ_i, $i = 1,2,3$ of the MZI loops, while the transparencies of the BS remain constant:

$$
\begin{aligned}
\theta_1 = \pi/8, \quad &\theta_1' = \pi/8, \quad \Phi_1 = -\pi/2, \quad \Phi_1' = \pi/2, \\
\theta_2 = \pi/4, \quad &\theta_2' = \pi/4, \quad \Phi_2 = \pi, \quad \Phi_2' = \pi/2, \\
\theta_3 = \pi/8, \quad &\theta_3' = \pi/8, \quad \Phi_3 = -\pi/2, \quad \Phi_3' = \pi/2.
\end{aligned}
\tag{32}
$$

Here we stress that the Φ phases presented in the last formula are "effective," meaning that they depend on the practical implementation of the BSs [values in the formula are for T given by Eq. (1)]. In Appendix B we show how to adjust the phases in the case of real experiments. This constitutes the justification for removing the additional loop in each MZ. The whole set of measurement schemes with $B = 4$ is presented in Appendix D.

VI. SETUP IN THE IQHE

While the setups which we have presented and discussed in this work were schematic, we think that a practical implementation is within reach with current experimental techniques. Using edge states in the IQHE regime, one can obtain chiral channels where backscattering is impossible. BSs can be obtained using quantum point contact. Several experiments realizing one or two electronic MZIs have already been achieved.[28]

The actual geometry for a working device, reproducing the setup in Fig. 1, is shown in Fig. 5. This figure represents a three-dimensional potential landscape. Lines going near the potential walls represent chiral edge eigenstates in the IQHE. Dotted lines represent unoccupied edge states. The Fermi sea is expelled from the setup region to prevent screening effects and parasitic entanglement. The edge states meet at quantum point contacts, whose transparency can be controlled by gate voltages. Each MZI has two electronic sources (labeled S_i and S_i', $i = 1,2,3$, in Fig. 5) and two drains collecting the electronic
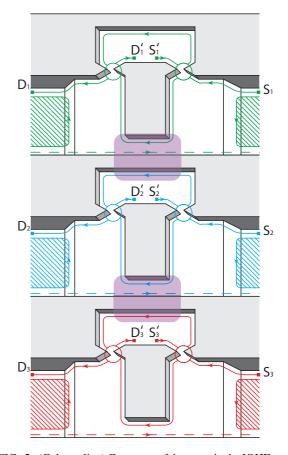

FIG. 5. (Color online) Geometry of the setup in the IQHE regime. S_j and S_j' ($j = 1,2,3$) are electron sources and D_j and D_j' are drains. Guiding centers of electron edge states meet at quantum point contacts, whose transparency can be controlled with gate voltages. The rounded rectangles indicate the interaction regions between neighboring MZIs. Space available for the Fermi sea is within the hatched regions.

current(D_i and D_i'). Note that by changing the gate voltages, it is possible to modulate the length of the different paths and, thus, to control the AB phase acquired by the electrons during propagation. The two rounded rectangles in the pictures show the interaction regions, where two branches of two different MZIs are put close to each other, in such a way that a π phase shift is produced when electrons are present in the two branches.

In order to have time-correlated propagation of electrons over interaction regions, we need on-demand electron sources similar to the ones which have already been experimentally realized in the IQHE.[27,29] In experiments on single-electron injection, the time of injection varied from 10^{-10} to 10^{-8} s (in this paragraph we use numerical values from Refs. 27–29). The wave packets should be shorter than the length of the interaction region. The mall size of wave packets ensures that the interaction produces a simple phase shift of the whole wave packet (see Appendix E). The suitable interaction time t then should be at least 10 times larger (more detailed calculations in the case of two MZIs are presented in Ref. 22) and starts with 10^{-9} s. The phase accumulated due to the interaction must be equal to π. For this to happen the interaction strength must exceed $U = \frac{h}{2t} \approx 3.3 \times 10^{-25}$ J. The unscreened Coulomb

interaction $\frac{e^2}{\epsilon r}$ ($\epsilon \approx 12$ is the dielectric constant of GaAs) provides such a strength at distances starting at 6.4×10^{-5} m, which is about 10^4 of the magnetic length $l_H \approx 10^{-8}$ m for a magnetic field $B = 5$ T. If the Fermi sea regions and various gates are at a distance larger than the distance between the edge states in the interaction region, using the unscreened form of the Coulomb interaction looks reasonable. Therefore the needed phase accumulation is accessible in realistic structures. If one uses short electron wave packets, another demand appears. As short packets have a wide energy distribution we must ensure that BS scattering is energy independent within that range. The energy width of a wave packet with duration 10^{-10} s is approximately 10 μeV. This requires a short enough scattering structure (e.g., quantum point contact) in the BS. The next issue is the size of the setup. If the interaction time equals 10^{-9} s, then for a drift velocity of 10^4–10^5 ms^{-1} (taken from Ref. 35), the interaction region length would be 10^{-5}–10^{-4} m. This length exceeds the size of electronic MZIs, where AB oscillations were observed. A satisfactory length for the interaction region should be of order 10^{-6} m. To achieve this length one may either produce shorter wave packets (keeping in mind that the BSs should remain energy independent) or reduce the drift velocity via making the potential walls smoother. Another issue is the accuracy of the interaction phases. First, one can tune the interaction strength with extra gates. If there is no such possibility, the setup should be fabricated with an interaction producing a phase shift exceeding π. Electrons then should be sent with a delay between them to reduce the interaction time and strength. The procedure for phase control may be developed in the same style as the AB-phase adjustment described in Appendix B. One should tune the bottom BS in the second MZI to transfer incoming electrons to the adjacent edge state and set the AB phase in the first MZI to 0. The interaction strength then should be tuned to the point where the electron sent to the first MZI comes out from a different lead. After this, for better tuning one applies an AB phase $\pi/2$. Here if the Coulomb interaction phase is equal to π, the sensitivity of one-particle probabilities in the first MZI reaches its maximum. Then the same procedure should be repeated for the second interaction zone. Although it appears to be possible to meet the requirements listed above, the realization of the experiment remains very challenging. It might therefore be very interesting to realize a less ambitious project with a constant voltage and detection of low-frequency third-order current-current correlator. The latter substitutes single-particle detection, while the former substitutes single-electron sources. One can also express orbital correlators, (30), in terms of current-current correlators (see Refs. 10 and 36). Third-order current correlation can be measured along the lines realized in Ref. 37 or theoretically suggested in Ref. 38. Still, in this case there is small hope for observation of Bell inequality violation, as it requires time-correlated propagation of electrons for accumulation of a definite phase (π) with the Coulomb interaction, which is a very rare event in the constant-voltage regime; the most probable event is no phase at all since electrons usually pass the interaction region separately. Therefore, in the constant-voltage regime the Bell inequlity violation paradigm becomes impractical and one has to come back to the usual physics and compare the experiment with some specific theory. This approach does not have the main advantage of Bell inequality violation, which indicates entanglement without addressing the details of the setup construction. Instead, one has to measure irreducible third-order current cross correlators as a function of interaction strength and other parameters (e.g., AB phases and BS transparencies). From that function it should be possible to find a term originating from the Coulomb interaction which would indirectly indicate entanglement. This kind of observation would also be a significant step towards the realization and detection of the GHZ state and electronic orbital states.

VII. CONCLUSION

In this article we have demonstrated how to produce a generalized GHZ state for three flying qubits, formed as orbital electron states in MZI-type geometries. Our setup relies on two state-of-the-art devices of nanophysics: (a) single-electron sources, which have been demonstrated[27] and characterized[29] experimentally, as well as theoretically;[32] and (b) MZIs, which have equally been the object of thorough experimental[28] and theoretical[33,34] investigations. In our proposal, both devices should be integrated together, and moreover, three MZIs placed in parallel are needed to achieve the GHZ state. While it is plausible to think that it will be challenging to build a prototype in the near-future, we judge that it is useful for the mesoscopic physics community to be aware that advanced quantum information protocols—here the production of a GHZ state—can be achieved with electrons.

At the beginning of the paper we justified that our ideal devices generate the GHZ state. Subsequently, we provided a detailed explanation of the type of Bell inequalities which need to be used to prove unambiguously that we have generated the proper state. The problem which we encountered with the actual MZI setup which is needed to implement the Bell test is that it requires three more MZI loops than the "condensed scheme," thus making the integration of the device even more challenging. Fortunately, we provided a "condensed detector scheme" where this complication can be circumvented, arguing that the operations achieved by two BSs in series can be combined with a single BS. This allowed us to actually draw a "realistic" device inspired from the so-called "air bridge" technique which is used in the experiments in Ref. 28.

This work thus belongs to the ongoing effort called "electron quantum optics" where experiments and paradigms of quantum optics are reproduced with mesoscopic physics devices. The great advantage of the present method for producing GHZ states lies in the fact that no postselection procedure is needed here. The steps described in this paper rely on a unitary evolution of the initial state, and moreover, we exploit the Coulomb interaction between electron wave packets in order to generate the desired phase shift in the electron wave function. This particular feature departs strongly from the photon protocols, as photons interact weakly when traveling in vacuum. We thus state that the use of electron-electron interactions in single-electron devices schemes may open up new possibilities for quantum information schemes which are not envisionable for photons.

Granted, the present work has addressed the case of an ideal device which is free from dephasing effects. Such phenomena are likely to affect the operation of our device, as they are already known to be present in single-MZI electronic setups.[33] Nevertheless, our top priority is to clarify how to implement an abstract quantum information scheme in an actual mesoscopic device. Our analysis could be refined by taking dephasing effects into account. The authors plan to consider this in the future. In the case of a similar scheme with two MZIs this is done in Ref. [22]. Also, we have pointed out some factors that need to be accounted for in experiments and mentioned a simplified scheme with a constant voltage instead of on-demand electron sources.

APPENDIX A: GHZ MAXIMAL VIOLATION PARAMETERS

Here we prove that in the tripartite case $B = 4$ can be achieved only for the GHZ state or states that can be reduced to GHZ with some local unitary transformations. Next we find all possible series of measurement angles which give $B = 4$ for the GHZ state. We use the spin-based approach in this section for convenience.

First, we compute the square of the Bell operator, (24), and find the conditions necessary for $\langle \hat{B}^2 \rangle = 16$:

$$\hat{B}^2 = 4 - [\hat{\sigma}_{\mathbf{a}_1}, \hat{\sigma}_{\mathbf{a}_1'}] \otimes [\hat{\sigma}_{\mathbf{a}_2}, \hat{\sigma}_{\mathbf{a}_2'}] \otimes \mathbf{1} \\ - \mathbf{1} \otimes [\hat{\sigma}_{\mathbf{a}_2}, \hat{\sigma}_{\mathbf{a}_2'}] \otimes [\hat{\sigma}_{\mathbf{a}_3}, \hat{\sigma}_{\mathbf{a}_3'}] \\ - [\hat{\sigma}_{\mathbf{a}_1}, \hat{\sigma}_{\mathbf{a}_1'}] \otimes \mathbf{1} \otimes [\hat{\sigma}_{\mathbf{a}_3}, \hat{\sigma}_{\mathbf{a}_3'}]. \quad (A1)$$

Pauli matrices ($i, j, k = x, y, z$) obey angular momentum commutation relations,

$$[\sigma_i, \sigma_j] = 2i\epsilon^{ijk}\sigma_k, \quad (A2)$$

from which we obtain the commutator for a spin pointing along arbitrary vectors $\mathbf{c}$ and $\mathbf{d}$,

$$[\sigma_{\mathbf{c}}, \sigma_{\mathbf{d}}] = 2i|\mathbf{e}|\sigma_{\mathbf{e}}, \quad (A3)$$

where $\mathbf{e} = \mathbf{c} \times \mathbf{d}$. For our task we need vectors $\mathbf{f}_1 = \mathbf{a}_1 \times \mathbf{a}_1'$, $\mathbf{f}_2 = \mathbf{a}_2 \times \mathbf{a}_2'$, $\mathbf{f}_3 = \mathbf{a}_3 \times \mathbf{a}_3'$. They allow us to represent $\hat{B}^2$ in the following form:

$$\hat{B}^2 = 4\big(1 + |\mathbf{f}_1||\mathbf{f}_2|\sigma_{\mathbf{f}_1} \otimes \sigma_{\mathbf{f}_2} \otimes \mathbf{1} + |\mathbf{f}_2||\mathbf{f}_3|\mathbf{1} \otimes \sigma_{\mathbf{f}_2} \otimes \sigma_{\mathbf{f}_3} \\ + |\mathbf{f}_1||\mathbf{f}_3|\sigma_{\mathbf{f}_1} \otimes \mathbf{1} \otimes \sigma_{\mathbf{f}_3}\big). \quad (A4)$$

This operator has a maximum eigenvalue $B^2 = 4(1 + |\mathbf{f}_1||\mathbf{f}_2| + |\mathbf{f}_2||\mathbf{f}_3| + |\mathbf{f}_1||\mathbf{f}_3|) \leqslant 4(1 + 1 + 1 + 1) = 16$.

For the maximum value to be achieved we require that $|\mathbf{f}_1| = |\mathbf{f}_2| = |\mathbf{f}_3| = 1$, which implies $\mathbf{a}_1 \perp \mathbf{a}_1'$, $\mathbf{a}_2 \perp \mathbf{a}_2'$, $\mathbf{a}_3 \perp \mathbf{a}_3'$. The eigenstates Ψ of this value obey the relations

$$\sigma_{\mathbf{f}_1} \otimes \sigma_{\mathbf{f}_2} \otimes \mathbf{1}\Psi = \Psi, \quad \mathbf{1} \otimes \sigma_{\mathbf{f}_2} \otimes \sigma_{\mathbf{f}_3}\Psi = \Psi, \\ \sigma_{\mathbf{f}_1} \otimes \mathbf{1} \otimes \sigma_{\mathbf{f}_3}\Psi = \Psi. \quad (A5)$$

It is convenient to choose a basis in each particle's space in relation to the corresponding f vector. For example, $|\uparrow\rangle$ for the first spin means that $\hat{\sigma}_{\mathbf{f}_1}|\uparrow\rangle = |\uparrow\rangle$. In this basis the only states which give $B^2 = 16$ are $|\uparrow\uparrow\uparrow\rangle$ and $|\downarrow\downarrow\downarrow\rangle$, so in full generality we choose a superposition:

$$\Psi = a|\uparrow\uparrow\uparrow\rangle + b|\downarrow\downarrow\downarrow\rangle. \quad (A6)$$

We can now find which state of the form of Eq. (A6) is an eigenstate of operator $\hat{B}$ with eigenvalue $B = 4$. Choosing the basis we associate the $\hat{z}$ axis of the first spin space with vector $\mathbf{f}_1$, and similarly for the other two spin states. This implies that $\mathbf{a}_1$ and $\mathbf{a}_1'$ are orthogonal vectors in the $\hat{x} - \hat{y}$ plane, and similarly for $\mathbf{a}_2$, $\mathbf{a}_2'$ and for $\mathbf{a}_3$, $\mathbf{a}_3'$. For specificity we choose $\mathbf{a}_1 \equiv \hat{x}$ and $\mathbf{a}_1' \equiv \hat{y}$, and analogously for the other spin components. Note that

$$\sigma_{\mathbf{a}_1'}\sigma_{\mathbf{a}_2}\sigma_{\mathbf{a}_3}|\uparrow\uparrow\uparrow\rangle = \sigma_{\mathbf{a}_1}\sigma_{\mathbf{a}_2'}\sigma_{\mathbf{a}_3}|\uparrow\uparrow\uparrow\rangle = \sigma_{\mathbf{a}_1}\sigma_{\mathbf{a}_2}\sigma_{\mathbf{a}_3'}|\uparrow\uparrow\uparrow\rangle \\ = -\sigma_{\mathbf{a}_1'}\sigma_{\mathbf{a}_2'}\sigma_{\mathbf{a}_3'}|\uparrow\uparrow\uparrow\rangle = i|\downarrow\downarrow\downarrow\rangle, \\ \sigma_{\mathbf{a}_1'}\sigma_{\mathbf{a}_2}\sigma_{\mathbf{a}_3}|\downarrow\downarrow\downarrow\rangle = \sigma_{\mathbf{a}_1}\sigma_{\mathbf{a}_2'}\sigma_{\mathbf{a}_3}|\downarrow\downarrow\downarrow\rangle = \sigma_{\mathbf{a}_1}\sigma_{\mathbf{a}_2}\sigma_{\mathbf{a}_3'}|\downarrow\downarrow\downarrow\rangle \\ = -\sigma_{\mathbf{a}_1'}\sigma_{\mathbf{a}_2'}\sigma_{\mathbf{a}_3'}|\downarrow\downarrow\downarrow\rangle = -i|\uparrow\uparrow\uparrow\rangle, \quad (A7)$$

thus implying that

$$\hat{B}(a|\uparrow\uparrow\uparrow\rangle + b|\downarrow\downarrow\downarrow\rangle) = -4ib|\uparrow\uparrow\uparrow\rangle + ia|\downarrow\downarrow\downarrow\rangle). \quad (A8)$$

From this we easily confirm that when $b = ia$ we have the desired eigenstate with $B = 4$:

$$\Psi = \frac{1}{\sqrt{2}}(|\uparrow\uparrow\uparrow\rangle + i|\downarrow\downarrow\downarrow\rangle). \quad (A9)$$

Also, note that the orthogonal state $\Psi' = \frac{1}{\sqrt{2}}(|\uparrow\uparrow\uparrow\rangle - i|\downarrow\downarrow\downarrow\rangle)$ has an eigenvalue $B = -4$. Both states are equivalent to the GHZ state up to local unitary transformations. In conclusion, we have shown that each state which can violate the Bell-type inequality maximally is a GHZ state up to trivial transformations.

Now we proceed with the reverse problem. Starting from the GHZ state, let us find all sets of vectors $\mathbf{a}_1, \mathbf{a}_2, \mathbf{a}_3, \mathbf{a}_1', \mathbf{a}_2', \mathbf{a}_3'$ which yield $\bar{B} = 4$. We consider a spin correlator $\langle \hat{\sigma}_{\mathbf{n}_1} \otimes \hat{\sigma}_{\mathbf{n}_2} \otimes \hat{\sigma}_{\mathbf{n}_3} \rangle$ for arbitrary unitary vectors $\mathbf{n}_1, \mathbf{n}_2, \mathbf{n}_3$ with corresponding spherical coordinates $\theta_{\mathbf{n}_1}, \phi_{\mathbf{n}_1}, \theta_{\mathbf{n}_2}, \phi_{\mathbf{n}_2}, \theta_{\mathbf{n}_3}, \phi_{\mathbf{n}_3}$.

The operator for the spin projection in direction $\mathbf{n}$ is then

$$\hat{\sigma}_{\mathbf{n}} = n_x\hat{\sigma}_x + n_y\hat{\sigma}_y + n_z\hat{\sigma}_z = \begin{pmatrix} \cos\theta_{\mathbf{n}} & \sin\theta_{\mathbf{n}}e^{-i\phi_{\mathbf{n}}} \\ \sin\theta_{\mathbf{n}}e^{i\phi_{\mathbf{n}}} & -\cos\theta_{\mathbf{n}} \end{pmatrix}. \quad (A10)$$

This allows us to find

$$\hat{\sigma}_{\mathbf{n}_1} \otimes \hat{\sigma}_{\mathbf{n}_2} \otimes \hat{\sigma}_{\mathbf{n}_3}|\uparrow\uparrow\uparrow\rangle \\ = \cos\theta_{\mathbf{n}_1}\cos\theta_{\mathbf{n}_2}\cos\theta_{\mathbf{n}_3}|\uparrow\uparrow\uparrow\rangle \\ + \sin\theta_{\mathbf{n}_1}\sin\theta_{\mathbf{n}_2}\sin\theta_{\mathbf{n}_3}e^{i(\phi_{\mathbf{n}_1}+\phi_{\mathbf{n}_2}+\phi_{\mathbf{n}_3})}|\downarrow\downarrow\downarrow\rangle + \cdots, \quad (A11)$$

$$\hat{\sigma}_{\mathbf{n}_1} \otimes \hat{\sigma}_{\mathbf{n}_2} \otimes \hat{\sigma}_{\mathbf{n}_3}|\downarrow\downarrow\downarrow\rangle \\ = \sin\theta_{\mathbf{n}_1}\sin\theta_{\mathbf{n}_2}\sin\theta_{\mathbf{n}_3}e^{-i(\phi_{\mathbf{n}_1}+\phi_{\mathbf{n}_2}+\phi_{\mathbf{n}_3})}|\uparrow\uparrow\uparrow\rangle \\ - \cos\theta_{\mathbf{n}_1}\cos\theta_{\mathbf{n}_2}\cos\theta_{\mathbf{n}_3}|\downarrow\downarrow\downarrow\rangle + \cdots, \quad (A12)$$

and the average of the spin correlator in the GHZ state is then

$$\langle \hat{\sigma}_{\mathbf{n_1}} \otimes \hat{\sigma}_{\mathbf{n_2}} \otimes \hat{\sigma}_{\mathbf{n_3}} \rangle = \sin \theta_{\mathbf{n_1}} \sin \theta_{\mathbf{n_2}} \sin \theta_{\mathbf{n_3}} \cos \left(\phi_{\mathbf{n_1}} + \phi_{\mathbf{n_1}} + \phi_{\mathbf{n_3}} \right).$$

$$(A13)$$

The simple formula which we have obtained is a justification of the spin-based approach to Bell-stype inequalities. The tripartite case is simpler than the bipartite state when it comes to finding the specific angles giving the Tsirel'son bound, since here all the correlators should have unit absolute value. This implies

$$\sin \theta_{\mathbf{n_1}} = \sin \theta_{\mathbf{n_2}} = \sin \theta_{\mathbf{n_3}} = 1, \qquad (A14)$$

and thus we should consider only vectors of the $\hat{x}$-$\hat{y}$ plane as candidates for $B = 4$. The polar angles of these vectors $\mathbf{a_1}$, $\mathbf{a_2}$, $\mathbf{a_3}$, $\mathbf{a'_1}$, $\mathbf{a'_2}$, $\mathbf{a'_3}$ are defined by the conditions

$$\langle \hat{\sigma}_{\mathbf{a'_1}} \otimes \hat{\sigma}_{\mathbf{a_2}} \otimes \hat{\sigma}_{\mathbf{a_3}} \rangle = 1, \quad \langle \hat{\sigma}_{\mathbf{a_1}} \otimes \hat{\sigma}_{\mathbf{a'_2}} \otimes \hat{\sigma}_{\mathbf{a_3}} \rangle = 1,$$
$$\langle \hat{\sigma}_{\mathbf{a_1}} \otimes \hat{\sigma}_{\mathbf{a_2}} \otimes \hat{\sigma}_{\mathbf{a'_3}} \rangle = 1, \quad \langle \hat{\sigma}_{\mathbf{a'_1}} \otimes \hat{\sigma}_{\mathbf{a'_2}} \otimes \hat{\sigma}_{\mathbf{a'_3}} \rangle = -1,$$

$$(A15)$$

which, in terms of polar angles, reads

$$\cos \left(\phi_{\mathbf{a'_1}} + \phi_{\mathbf{a_2}} + \phi_{\mathbf{a_3}} \right) = 1, \quad \cos \left(\phi_{\mathbf{a_1}} + \phi_{\mathbf{a'_2}} + \phi_{\mathbf{a_3}} \right) = 1,$$
$$\cos \left(\phi_{\mathbf{a_1}} + \phi_{\mathbf{a_2}} + \phi_{\mathbf{a'_3}} \right) = 1, \quad \cos \left(\phi_{\mathbf{a'_1}} + \phi_{\mathbf{a'_2}} + \phi_{\mathbf{a'_3}} \right) = -1.$$

$$(A16)$$

This system of equations has the solution

$$\phi_{\mathbf{a_1}} + \phi_{\mathbf{a_2}} + \phi_{\mathbf{a_3}} = \pm \frac{\pi}{2}, \qquad (A17)$$

with $\phi_{\mathbf{a'_i}} = \phi_{\mathbf{a_i}} \mp \pi/2$, where $i = 1,2,3$. All the vectors lie in the $\hat{x}$-$\hat{y}$ plane.

This concludes the definition of the angles giving $B = 4$ for the GHZ state.

APPENDIX B: BEAM-SPLITTER PARAMETRIZATION

One of the essential parts of the device is the BS. The BS is a four-arm scatterer with a special type of scattering matrix which allows us to split the beam into two parts without any reflection. Generally the scattering matrix of a four-arm splitter looks like

$$S = \begin{pmatrix} r_{11} & t_{21} & t_{31} & t_{41} \\ t_{12} & r_{22} & t_{32} & t_{42} \\ t_{13} & t_{23} & r_{33} & t_{43} \\ t_{14} & t_{24} & t_{34} & r_{44} \end{pmatrix}. \qquad (B1)$$

In this matrix the t_{ij} parameters refer to the transmission amplitudes from arm j to arm i, and r_{ii} is the reflection amplitude in arm i. This matrix obeys only a unitarity condition. If time-reversal invariance is added, a new condition appears: $t_{ij} = t_{ji}$. The BS scattering matrix is

$$S = \begin{pmatrix} 0 & 0 & t_{31} & t_{41} \\ 0 & 0 & t_{32} & t_{42} \\ t_{31} & t_{32} & 0 & 0 \\ t_{41} & t_{42} & 0 & 0 \end{pmatrix}. \qquad (B2)$$

For these parameters the following system of equations is valid:

$$T_{31} + T_{41} = 1, \quad T_{31} + T_{32} = 1,$$
$$T_{32} + T_{42} = 1, \quad t_{31}t_{32}^* + t_{41}t_{42}^* = 0,$$

$$(B3)$$

where $T_{ij} = |t_{ij}|^2$. For such an equation set it is rather easy to find a simple parametrization. Let us assume that $t_{31} = \cos \theta e^{i\phi_{31}}$, $t_{41} = \sin \theta e^{i\phi_{41}}$, $t_{32} = \sin \theta e^{i\phi_{32}}$, $t_{42} = \cos \theta e^{i\phi_{42}}$. Then we substitute all the t values into the last equation and get

$$\cos \theta \sin \theta e^{i\phi_{31}-i\phi_{32}} + \sin \theta \cos \theta e^{i\phi_{41}-i\phi_{42}} = 0. \qquad (B4)$$

For this equation to be valid the following must hold:

$$\phi_{31} - \phi_{32} - \phi_{41} + \phi_{42} = \pi + 2\pi n, \quad n \in \mathbb{Z}. \qquad (B5)$$

In the present work we focus on symmetrical BSs for simplicity. For a symmetrical BS

$$t_{31} = t_{42}, \quad t_{32} = t_{41}, \qquad (B6)$$

so the phases are $\phi_{31} = \phi_{42}$, $\phi_{32} = \phi_{41}$ and Eq. (B5) simplifies to

$$\phi_{31} - \phi_{32} = \pi/2 + \pi n, \quad n \in \mathbb{Z}. \qquad (B7)$$

One of the possible solutions is

$$\phi_{31} = 0, \quad t_{31} = t_{42} = \cos \theta,$$
$$\phi_{32} = \pi/2, \quad t_{32} = t_{41} = i \sin \theta.$$

$$(B8)$$

This parametrization is used in further calculations.

We are interested in the properties of electron transport from bottom to top, so we need only the values of t_{31}, t_{32}, t_{41}, and t_{42}. Now we can introduce the transfer matrix:

$$T = \begin{pmatrix} t_{RR} & t_{LR} \\ t_{RL} & t_{LL} \end{pmatrix} = \begin{pmatrix} i \sin\theta & \cos \theta \\ \cos \theta & i \sin\theta \end{pmatrix}. \qquad (B9)$$

Note that we have changed indices because of the reflectionless nature of the BS: $t_{RR} = t_{32}$, $t_{RL} = t_{42}$, $t_{LR} = t_{31}$, $t_{LL} = t_{31}$. In order to find the state of particles after the BS one must perform the following substitution with wave functions before the BS:

$$\psi_R \rightarrow \cos \theta \psi_L + i \sin \theta \psi_R,$$
$$\psi_L \rightarrow \cos \theta \psi_R + i \sin \theta \psi_L.$$

$$(B10)$$

Since we have chosen a specific parametrization of the BS, we must confirm that if the BS used in the experiment has a transfer matrix which is different from the one in Eq. (B9) it will not spoil the whole experiment.

We consider again the phase relation in the general case:

$$\phi_{31} - \phi_{32} - \phi_{41} + \phi_{42} = \pi + 2\pi n, \quad n \in \mathbb{Z}. \qquad (B11)$$

Each phase can be presented as

$$\phi_{31} = \tilde{\phi}_{31} + 2\pi n \equiv \tilde{\phi}_{31}, \quad \phi_{32} = \pi/2 + \tilde{\phi}_{32},$$
$$\phi_{41} = \pi/2 + \tilde{\phi}_{41}, \quad \phi_{42} = \tilde{\phi}_{42},$$

$$(B12)$$

where the phases $\tilde{\phi}_{31}$, $\tilde{\phi}_{32}$, $\tilde{\phi}_{41}$, $\tilde{\phi}_{42}$ represent the deviation from the chosen parametrization. These obey the relation

$$\tilde{\phi}_{31} - \tilde{\phi}_{32} - \tilde{\phi}_{41} + \tilde{\phi}_{42} = 0. \qquad (B13)$$
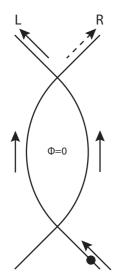
FIG. 6. For $\Phi = 0$ the electron goes to the left arm.

All solutions of this equation are taken into account by the following representation:

$$\tilde{\phi}_{31} = \phi_3, \quad \tilde{\phi}_{32} = \phi_3 + \phi_2, \quad \tilde{\phi}_{41} = \phi_4, \quad \tilde{\phi}_{42} = \phi_4 + \phi_2.$$
$$\text{(B14)}$$

where ϕ_2, ϕ_3, ϕ_4 are some real values.

This answer has an explicit physical meaning. All BSs have the same transfer matrix up to the phase accumulation in each channel. This phase accumulation can affect the phase difference in the left and the right paths of the MZI. In order to restore the original interference pattern we need to adjust the applied phase difference. During the experiment this means choosing a reference point with $\Phi = 0$ for a given MZI. This could be achieved using the fact that at $\Phi = 0$ an electron injected into the right arm of the MZI has zero probability of being detected in the right arm (Fig. 6). Even better tuning can be achieved near $\pi/2$. Here the probabilities for each arm are equal and the difference between the probabilities has a maximum derivative with respect to the phase.

1. Beam splitter with phase

In our MZI the electrons have two possible paths to travel. If there is a difference in the accumulated phase between two paths, it will affect the interference between them in a subsequent BS. It is convenient to account for this phase difference (which can be generated e.g. by applying a magnetic flux through the MZI loop) in the transfer matrix of the BS. If the phase lengths of the right and left the paths are ϕ_L and ϕ_R, then the transfer matrix of the BS takes the form

$$T = \begin{pmatrix} i\sin\theta e^{i\phi_R} & \cos\theta e^{i\phi_L} \\ \cos\theta e^{i\phi_R} & i\sin\theta e^{i\phi_L} \end{pmatrix}.$$
$$\text{(B15)}$$

Actually the final results depend only on the phase difference of the two paths $\Phi = \phi_L - \phi_R$, so the transfer matrix can be multiplied by any phase factor without affecting the final results. We can represent the transfer matrix in a form similar

to the spin rotation operator:

$$T = \begin{pmatrix} \sin\theta e^{-i\Phi/2} & -i\cos\theta e^{i\Phi/2} \\ -i\cos\theta e^{-i\Phi/2} & \sin\theta e^{i\Phi/2} \end{pmatrix} = e^{-i\sigma_x \frac{(\pi-2\theta)}{2}} e^{-i\sigma_z \frac{\Phi}{2}}.$$
$$\text{(B16)}$$

Since the measurement procedure in the condensed scheme includes changing θ and Φ and measuring $\langle \sigma_z \otimes \sigma_z \otimes \sigma_z \rangle$ at level lv2′ (Fig. 1), it is convenient to define a measurement operator with respect to level lv2 in the scheme, where the electron state is invariant during the measurement procedure.

As we see, the operator is a sum of two rotations: first, a rotation of angle Φ around the z axis and. second, another rotation of angle $\pi - 2\theta$ around the x axis. The rotation around the x axis corresponds to the action of the BS itself, while the rotation around z corresponds to an AB phase accumulation. This whole rotation transforms a vector,

$$\mathbf{n} = \begin{pmatrix} \sin 2\theta \sin \Phi \\ \sin 2\theta \cos \Phi \\ -\cos 2\theta \end{pmatrix},$$
$$\text{(B17)}$$

onto the z axis. As the vector thus defined is in one-to-one correspondence with the pair of BS parameters θ, Φ, we call it a characteristic vector of the BS. Rotation means that

$$T|\mathbf{n}\rangle = U_{\mathbf{n}\to z}|\mathbf{n}\rangle = |\uparrow\rangle.$$
$$\text{(B18)}$$

The projection of the rotated pseudospin onto z can be shown to be equal to the projection of the initial pseudospin onto $\mathbf{n}$:

$$\langle U_{\mathbf{n}\to z}\Psi|\sigma_z|U_{\mathbf{n}\to z}\Psi\rangle = \langle\Psi|U_{\mathbf{n}\to z}^+\sigma_z U_{\mathbf{n}\to z}|\Psi\rangle = \langle\Psi|\sigma_{\mathbf{n}}|\Psi\rangle.$$
$$\text{(B19)}$$

For three-particle spin correlators the same relation holds:

$$\langle T_1 \otimes T_2 \otimes T_3 \Psi | \sigma_z \otimes \sigma_z \otimes \sigma_z | T_1 \otimes T_2 \otimes T_3 \Psi \rangle$$
$$= \langle \Psi | T_1^+ \sigma_z T_1 \otimes T_2^+ \sigma_z T_2 \otimes T_3^+ \sigma_z T_3 | \Psi \rangle$$
$$= \langle \Psi | \sigma_{\mathbf{n_1}} \otimes \sigma_{\mathbf{n_2}} \otimes \sigma_{\mathbf{n_3}} | \Psi \rangle.$$
$$\text{(B20)}$$

So now we have found that the measured correlator with respect to level lv2 is $\langle \sigma_{\mathbf{n_1}} \otimes \sigma_{\mathbf{n_2}} \otimes \sigma_{\mathbf{n_3}} \rangle$.

APPENDIX C: PSEUDOSPIN ANALOGY

In Appendix A we have defined angles yielding $B = 4$ for the three-spin GHZ state. To obtain the parameters of the actual setup (Fig. 1) we need to "translate" the spin angles into BS parameters. This chapter contains the derivation of the "translation" rules.

We start with the logic of the GHZ experiment described in Sec. III. We need three values, x_1, x_2, x_3, corresponding to separate measurements with results within the interval $[-1; 1]$. In the spin case, the spin projection measurements serve this purpose. In our setup we can detect a particle in the left or the right arm. So one of the possible assignments is $x = -1$ for a particle detected in the left arm and $x = 1$ for a particle detected in the right arm. Then the Bell correlator is

$$\langle x_1 x_2 x_3 \rangle = P_{RRR} + P_{RLL} + P_{LRL} + P_{LLR}$$
$$- P_{LLL} - P_{LRR} - P_{RLR} - P_{RRL}. \quad \text{(C1)}$$

This correlator measured on level lv3 of the setup (Fig. 1) corresponds to the $\langle \hat{\sigma}_z \otimes \hat{\sigma}_z \otimes \hat{\sigma}_z \rangle$ correlator of pseudospin.

Due to the rotation between lv2′ and level lv3, the correlator of Eq. (C1) corresponds to the $\langle \hat{\sigma}_{\mathbf{n_1}} \otimes \hat{\sigma}_{\mathbf{n_2}} \otimes \hat{\sigma}_{\mathbf{n_3}} \rangle$ measured for the initial pseudospin state at lv2′, which is the GHZ. The vectors $\mathbf{n_1}$, $\mathbf{n_2}$, $\mathbf{n_3}$ are characteristic vectors of the corresponding BSs, (B17).

Now we calculate BS matrices corresponding to the angles giving maximum violation, (A17). All the vectors are in the $\hat{x}$-$\hat{y}$ plane, thus $\theta = \pi/4$ for all of them. For a vector with a polar angle ϕ, correspondingly, $\Phi = \alpha = \pi/2 - \phi$ and the BS transfer matrix is

$$T(\alpha) = \begin{pmatrix} \frac{1}{\sqrt{2}}e^{-i\alpha/2} & -\frac{i}{\sqrt{2}}e^{i\alpha/2} \\ -\frac{i}{\sqrt{2}}e^{-i\alpha/2} & \frac{1}{\sqrt{2}}e^{i\alpha/2} \end{pmatrix} \equiv \begin{pmatrix} \frac{i}{\sqrt{2}} & \frac{1}{\sqrt{2}}e^{i\alpha} \\ \frac{1}{\sqrt{2}} & \frac{i}{\sqrt{2}}e^{i\alpha} \end{pmatrix},$$
(C2)

where equivalence means that the overall phase does not change the observable outcomes. α parameters then should obey the restrictions

$$\alpha_{\mathbf{a_1}} + \alpha_{\mathbf{a_2}} + \alpha_{\mathbf{a_3}} = \pi/2 \pm \pi/2, \quad \alpha_{\mathbf{a_i'}} = \alpha_{\mathbf{a_i}} \pm \pi/2, \quad \text{(C3)}$$

for $i = 1,2,3$.

APPENDIX D: SETTINGS GIVING MAXIMUM VIOLATION OF THE BELL INEQUALITY

In Appendix C we have defined the properties of the BS between level lv2′ and level lv3 in Fig. 1. The next step lies in defining the parameters of the BS in the condensed scheme. For this purpose we use the properties of the unitary transformation made between level lv2 and lv2′ of the initial setup, (14).

The problem is simplified by the fact that all BSs between level lv2′ and level lv3 are of the same type:

$$T(\alpha) = \begin{pmatrix} \frac{i}{\sqrt{2}} & \frac{1}{\sqrt{2}}e^{i\alpha} \\ \frac{1}{\sqrt{2}} & \frac{i}{\sqrt{2}}e^{i\alpha} \end{pmatrix}.$$
(D1)

a. First and third MZIs

Since $U_3 = U_1$ all the results are valid for the third MZI as well. The first MZI chain makes two consequent unitary transformations; the first one is $U_1 = \frac{1}{\sqrt{2}}\begin{pmatrix} -i & 1 \\ 1 & -i \end{pmatrix}$, and the next is $T(\alpha) = \frac{1}{\sqrt{2}}\begin{pmatrix} i & e^{i\alpha} \\ 1 & ie^{i\alpha} \end{pmatrix}$. The product of these is unitary:

$$T_1(\alpha) = T(\alpha)U_1 = \frac{1}{2}\begin{pmatrix} 1+e^{i\alpha} & i-ie^{i\alpha} \\ -i+ie^{i\alpha} & 1+e^{i\alpha} \end{pmatrix}.$$
(D2)

Shifting the whole matrix phase by $-\alpha/2$ we get the following expression:

$$T_1(\Phi) = \begin{pmatrix} \cos(\alpha/2) & \sin(\alpha/2) \\ -\sin(\alpha/2) & \cos(\alpha/2) \end{pmatrix}.$$
(D3)

The next step is to find from the matrix of the BS the parameters θ, Φ. We encounter the problem that the matrix of Eq. (D3) cannot represent the transfer matrix of any BS. The relation $\arg(t_{RR}/t_{RL}) = \frac{\pi}{2}$, which is universal for any representation of the transfer matrix [see Eq. (B15)], is not valid for Eq. (D3). The BS transfer matrix should not necessarily be equal to $T_1(\Phi)$ but it should lead to the same three-particle probabilities.

This happens if the transfer matrix of the BS equals

$$T_1(\Phi,\phi_1,\phi_2) = \begin{pmatrix} \cos(\alpha/2)e^{i\phi_1} & \sin(\alpha/2)e^{i\phi_1} \\ -\sin(\alpha/2)e^{i\phi_2} & \cos(\alpha/2)e^{i\phi_2} \end{pmatrix}, \quad \text{(D4)}$$

where ϕ_1 and ϕ_2 are some phase shifts. They do not contribute to the tripartite probabilities, while this matrix with properly chosen phase shifts can be the transfer matrix of the BS.

If $\tan(\alpha/2) > 0$, then $\phi_1 = \pi/2$, $\phi_2 = \pi$, and

$$\theta = \frac{\pi - \alpha}{2}, \quad \Phi = \frac{\pi}{2}.$$
(D5)

If $\tan(\alpha/2) < 0$, then $\phi_1 = \pi/2$, $\phi_2 = 0$, and

$$\theta = \frac{\pi + \alpha}{2}, \quad \Phi = -\frac{\pi}{2}.$$
(D6)

Both formulas can be unified as

$$\theta = \frac{\pi - \text{sign}\tan(\alpha/2)\alpha}{2}, \quad \Phi = \text{sign}\tan(\alpha/2)\frac{\pi}{2}. \quad \text{(D7)}$$

If $\alpha \in [-\pi;\pi]$, the last formula is simplified:

$$\theta = \frac{\pi - |\alpha|}{2}, \quad \Phi = \frac{\pi|\alpha|}{2\alpha}.$$
(D8)

b. Second MZI

For the second MZI everything is simpler since U_2 is a diagonal matrix:

$$T_2(\alpha) = T(\alpha)U_2 = \frac{1}{\sqrt{2}}\begin{pmatrix} -1 & e^{i\alpha} \\ i & ie^{i\alpha} \end{pmatrix} \equiv \frac{1}{\sqrt{2}}\begin{pmatrix} i & e^{i(\alpha-\pi/2)} \\ 1 & ie^{i(\alpha-\pi/2)} \end{pmatrix}.$$
(D9)

This matrix corresponds to a BS with parameters $\theta = \pi/4$ and $\Phi = \alpha - \pi/2$.

Finally, we can introduce the algorithm for the generation of the measurement settings resulting in $B = 4$.

(1) Choose angles $\alpha_{\mathbf{a_1}}$, $\alpha_{\mathbf{a_2}}$, $\alpha_{\mathbf{a_3}}$ obeying relations

$$\alpha_{\mathbf{a_1}} + \alpha_{\mathbf{a_2}} + \alpha_{\mathbf{a_3}} = \pi/2 \pm \pi/2, \quad \alpha_{\mathbf{a_i'}} = \alpha_{\mathbf{a_i}} \pm \pi/2, \quad \text{(D10)}$$

where $i = 1,2,3$.

(2) Make $\alpha_{\mathbf{a_i}}, \alpha_{\mathbf{a_i'}}$ be within $[-\pi;\pi]$ by applying $2\pi n, n \in \mathbb{Z}$ shifts if needed.

(3) Calculate the BS parameters:

$$\theta_{1,3} = \frac{\pi - |\alpha_{\mathbf{a_{1,3}}}|}{2}, \quad \theta_{1,3}' = \frac{\pi - |\alpha_{\mathbf{a_{1,3}'}}|}{2},$$

$$\Phi_{1,3} = \frac{\pi|\alpha_{\mathbf{a_{1,3}}}|}{2\alpha_{\mathbf{a_{1,3}}}}, \quad \Phi_{1,3}' = \frac{\pi|\alpha_{\mathbf{a_{1,3}'}}|}{2\alpha_{\mathbf{a_{1,3}'}}},$$

$$\theta_2 = \pi/4, \quad \theta_2' = \pi/4,$$

$$\Phi_2 = \alpha_{\mathbf{a_2}} - \pi/2, \quad \Phi_2' = \alpha_{\mathbf{a_2'}} - \pi/2.$$
(D11)

From the last equation we can extract the following common features of these measurement sets:

(a) In the first and the third MZIs the AB phase can take values $\pm\pi/2$;

(b) In the second MZI the transparency of the BS does not change during the experiment.

Among the measurement schemes there exist ones where the transparencies of all BS do not change during the experiment. For example, choosing

$$\alpha_{\mathbf{a}_1} = -3\pi/4, \quad \alpha_{\mathbf{a}_1'} = 3\pi/4,$$
$$\alpha_{\mathbf{a}_2} = -\pi/2, \quad \alpha_{\mathbf{a}_2'} = \pi, \tag{D12}$$
$$\alpha_{\mathbf{a}_3} = -3\pi/4, \quad \alpha_{\mathbf{a}_3'} = 3\pi/4,$$

we get

$$\theta_1 = \pi/8, \quad \theta_1' = \pi/8, \quad \Phi_1 = -\pi/2, \quad \Phi_1' = \pi/2,$$
$$\theta_2 = \pi/4, \quad \theta_2' = \pi/4, \quad \Phi_2 = \pi, \quad \Phi_2' = \pi/2, \tag{D13}$$
$$\theta_3 = \pi/8, \quad \theta_3' = \pi/8, \quad \Phi_3 = -\pi/2, \quad \Phi_3' = \pi/2.$$

In conclusion, we have found the general parametrization for measurement settings giving $B = 4$ in a regular MZ setup and described a special case where we get a maximum violation only by adjusting the AB phases.

APPENDIX E: COULOMB INTERACTION

Here we solve the two-particle problem for the propagation of two electrons in neighboring channels between the two BSs. We consider two chiral edge channels of the IQHE. The two particles propagating in different channels interact electrostatically within a specified interaction region. The potential of the interaction $U(x_1, x_2)$ depends on the position of both particles. The energy spectrum is assumed to be linear and the drift velocity of the electrons in each channel is the same v_D. We consider the Hilbert space of two electron wave functions such that $\int \Psi(x_1, x_2) e^{-ik_1 x_1 - ik_2 x_2} dx_1 dx_2 = 0$ if k_1 or k_2 is negative. The Schrödinger equation for this two-particle problem reads

$$i \frac{\partial}{\partial t} \Psi(x_1, x_2, t) = \left(-iv_D \frac{\partial}{\partial x_1} - iv_D \frac{\partial}{\partial x_2} \right) \Psi(x_1, x_2, t)$$
$$+ U(x_1, x_2) \Psi(x_1, x_2, t). \tag{E1}$$

Let us make the substitution $a_\alpha = x_\alpha - v_F t$. Then $\Psi(x_1, x_2, t) = \Phi(a_1, a_2, t)$. Here

$$\frac{\partial}{\partial t} = \frac{\partial}{\partial t} + v_D \frac{\partial}{\partial x_1} + v_D \frac{\partial}{\partial x_2}, \tag{E2}$$

and this allows us to rewrite the equation,

$$\frac{\partial}{\partial t} \Phi = -iU(a_1 + v_D t, a_2 + v_D t)\Phi. \tag{E3}$$

The solution is

$$\Phi(a_1, a_2, t) = \Phi(a_1, a_2, 0) e^{-i \int_0^t U(a_1 + v_D \tau, a_2 + v_D \tau) d\tau}. \tag{E4}$$

In terms of the initial variables,

$$\Psi(x_1, x_2, t) = \Psi_0(x_1 - v_D t, x_2 - v_D t)$$
$$\times e^{-i \int_0^t U(x_1 + v_D(\tau - t), x_2 + v_D(\tau - t)) d\tau}. \tag{E5}$$

The phase accumulated during the interaction is position dependent and describes the energy exchange and the deformation of the wave packets. Here the condition for simple phase accumulation is that the size of the wave packets is small. In this case the position dependence of the phase should not manifest itself. The solution agrees well with the derivation in Ref. 23 except for the fact that the interaction kernel differs [we used a kernel of general form $U(x_1, x_2)$].

[1] A. Einstein, B. Podolsky, and N. Rosen, Phys. Rev. **47**, 777 (1935).

[2] E. Schrödinger, Naturwissenschaften **23**, 807 (1935).

[3] J. S. Bell, Phys. **1**, 195 (1964).

[4] J. F. Clauser, M. A. Horne, A. Shimony, and R. A. Holt, Phys. Rev. Lett. **23**, 880 (1969).

[5] A. Aspect, P. Grangier, and G. Roger, Phys. Rev. Lett. **47**, 460 (1981).

[6] G. Lesovik, T. Martin, and G. Blatter, Eur. Phys. J. B **24**, 287 (2001).

[7] P. Recher, E. V. Sukhorukov, and D. Loss, Phys. Rev. B **63**, 165314 (2001).

[8] C. W. J. Beenakker, C. Emary, M. Kindermann, and J. L. van Velsen, Phys. Rev. Lett. **91**, 147901 (2003).

[9] P. Samuelsson, E. V. Sukhorukov, and M. Büttiker, Phys. Rev. Lett. **91**, 157002 (2003); **92**, 026805 (2004).

[10] N. M. Chtchelkatchev, G. Blatter, G. B. Lesovik, and T. Martin, Phys. Rev. B **66**, 161320 (2002).

[11] A. V. Lebedev, G. B. Lesovik, and G. Blatter, Phys. Rev. B **71**, 045306 (2005).

[12] O. Sauret, T. Martin, and D. Feinberg, Phys. Rev. B **72**, 024544 (2005).

[13] K. V. Bayandin, G. B. Lesovik, and T. Martin, Phys. Rev. B **74**, 085326 (2006).

[14] D. M. Greenberger, M. A. Horne, A. Shimony, and A. Zeilinger, Am. J. Phys. **58**, 1131 (1990).

[15] B. S. Cirel'son, Lett. Math. Phys. **4**, 93 (1980).

[16] M. A. Nielsen and I. L. Chuang, *Quantum Computation and Quantum information* (Cambridge University Press, Cambridge, 2000).

[17] A. Karlsson and M. Bourennane, Phys. Rev. A **58**, 4394 (1998).

[18] J. C. Hao, C. F. Li, and G. C. Guo, Phys. Rev. A **63**, 054301 (2001).

[19] A. Zeilinger, M. A. Horne, H. Weinfurter, and M. Zukowski, Phys. Rev. Lett. **78**, 3031 (1997).

[20] A. V. Lebedev, G. Blatter, C. W. J. Beenakker, and G. B. Lesovik, Phys. Rev. B **69**, 235312 (2004)

[21] K. Kang and K. H. Lee, Physica E **40**, 1395 (2008).

[22] A. A. Vyshnevyy, A. V. Lebedev, G. B. Lesovik, and G. Blatter arXiv:1212.6924.

[23] J. Dressel, Y. Choi, and A. N. Jordan, Phys. Rev. B **85**, 045320 (2012).

[24] D. Bouwmeester, J.-W. Pan, M. Daniell, H. Weinfurter, and A. Zeilinger, Phys. Rev. Lett. **82**, 1345 (1999).

[25] C.-Y. Lu, X.-Q. Zhou, O. Gühne, W.-B. Gao, J. Zhang, Z.-S. Yuan, A. Goebel, T. Yang, and J.-W. Pan, Nature Phys. **3**, 91 (2007).

[26] L. M. K. Vandersypen, M. Steffen, G. Breyta, C. S. Yannoni, M. H. Sherwood, and I. L. Chuang, Nature **414**, 883 (2001).

[27] G. Fève *et al.*, Science **316**, 1169 (2007).

[28] Y. Ji, Y. Chung, D. Sprinzak, M. Heiblum, D. Mahalu, and H. Shtrikman, Nature **422**, 415 (2003); I. Neder, N. Ofek, Y. Chung, M. Heiblum, D. Mahalu, and V. Umansky, *ibid.* **448**, 333 (2007); P. Roulleau, F. Portier, D. C. Glattli, P. Roche, A. Cavanna, G. Faini, U. Gennser, and D. Mailly, Phys. Rev. B **76**, 161309 (2007).

[29] A. Mahé, F. D. Parmentier, E. Bocquillon, J.-M. Berroir, D. C. Glattli, T. Kontos, B. Placais, G. Fève, A. Cavanna, and Y. Jin, Phys. Rev. B **82**, 201309(R) (2010).

[30] G. B. Lesovik, M. V. Suslov, and G. Blatter, Phys. Rev. A **82**, 012316 (2010).

[31] A. V. Belinskii and D. N. Klyshko, Phys. Usp. **36**, 653 (1993).

[32] M. Albert, C. Flindt, and M. Büttiker, Phys. Rev. B **82**, 041407(R) (2010); Phys. Rev. Lett. **107**, 086805 (2011); G. Haack, M. Moskalets, J. Splettstoesser, and M. Büttiker, Phys. Rev. B **84**,

081303(R) (2011); T. Jonckheere, T. Stoll, J. Rech, and T. Martin, *ibid.* **85**, 045321 (2012).

[33] H. Forster, S. Pilgram, and M. Büttiker, Phys. Rev. B **72**, 075301 (2005); F. Marquardt, Europhys. Lett. **72**, 788 (2005); F. Marquardt and C. Bruder, Phys. Rev. Lett. **92**, 056805 (2004); S.-C. Youn, H.-W. Lee, and H.-S. Sim, *ibid.* **100**, 196807 (2008).

[34] D. L. Kovrizhin and J. T. Chalker, Phys. Rev. B **81**, 155318 (2010).

[35] P. Roulleau, F. Portier, P. Roche, A. Cavanna, G. Faini, U. Gennser, and D. Mailly, Phys. Rev. Lett. **101**, 186803 (2008).

[36] C. W. J. Beenakker, C. Emary, and M. Kindermann, Phys. Rev. B **69**, 115320 (2004).

[37] G. Gershon, Yu. Bomze, E. V. Sukhorukov, and M. Reznikov, Phys. Rev. Lett. **101**, 016803 (2008).

[38] K. V. Bayandin, A. V. Lebedev, and G. B. Lesovik, JETP **106**, 117 (2008).